

Quantum oscillations with magnetic hysteresis observed in CeTe_3 thin films

Cite as: Appl. Phys. Lett. **117**, 072403 (2020); <https://doi.org/10.1063/5.0007517>

Submitted: 13 March 2020 . Accepted: 03 August 2020 . Published Online: 19 August 2020

Mori Watanabe, Sanghyun Lee, Takuya Asano, Takashi Ibe, Masashi Tokuda, Hiroki Taniguchi, Daichi Ueta, Yoshinori Okada, Kensuke Kobayashi , and Yasuhiro Niimi 



View Online



Export Citation



CrossMark

ARTICLES YOU MAY BE INTERESTED IN

[A four-state magnetic tunnel junction switchable with spin-orbit torques](#)

Applied Physics Letters **117**, 072404 (2020); <https://doi.org/10.1063/5.0014771>

[Engineering the magnetocaloric properties of \$\text{PrVO}_3\$ epitaxial oxide thin films by strain effects](#)

Applied Physics Letters **117**, 072402 (2020); <https://doi.org/10.1063/5.0021031>

[Reconfigurable spin orbit logic device using asymmetric Dzyaloshinskii-Moriya interaction](#)

Applied Physics Letters **117**, 072401 (2020); <https://doi.org/10.1063/5.0020953>



Contact Hiden Analytical for further details:
www.HidenAnalytical.com
info@hiden.co.uk

[CLICK TO VIEW](#) our product catalogue

Instruments for Advanced Science



Gas Analysis

- dynamic measurement of reaction gas streams
- catalysis and thermal analysis
- molecular beam studies
- dissolved species probes
- fermentation, environmental and ecological studies




Surface Science

- UHV TPD
- SIMS
- end point detection in ion beam etch
- elemental imaging - surface mapping



Plasma Diagnostics

- plasma source characterization
- etch and deposition process reaction kinetic studies
- analysis of neutral and radical species



Vacuum Analysis

- partial pressure measurement and control of process gases
- reactive sputter process control
- vacuum diagnostics
- vacuum coating process monitoring

Quantum oscillations with magnetic hysteresis observed in CeTe₃ thin films

Cite as: Appl. Phys. Lett. **117**, 072403 (2020); doi: [10.1063/5.0007517](https://doi.org/10.1063/5.0007517)

Submitted: 13 March 2020 · Accepted: 3 August 2020 ·

Published Online: 19 August 2020



View Online



Export Citation



CrossMark

Mori Watanabe,¹ Sanghyun Lee,¹ Takuya Asano,¹ Takashi Ibe,¹ Masashi Tokuda,¹ Hiroki Taniguchi,¹ Daichi Ueta,² Yoshinori Okada,² Kensuke Kobayashi,^{1,3}  and Yasuhiro Niimi^{1,4,a)} 

AFFILIATIONS

¹Department of Physics, Graduate School of Science, Osaka University, Toyonaka, Osaka 560-0043, Japan

²Okinawa Institute of Science and Technology Graduate University, Okinawa 904-0495, Japan

³Institute for Physics of Intelligence and Department of Physics, The University of Tokyo, Bunkyo-ku, Tokyo 113-0033, Japan

⁴Center for Spintronics Research Network, Osaka University, Toyonaka, Osaka 560-8531, Japan

a) Author to whom correspondence should be addressed: niimi@phys.sci.osaka-u.ac.jp

ABSTRACT

We have performed magnetotransport measurements in CeTe₃ thin films down to 0.2 K. It is known that CeTe₃ has two magnetic transitions at $T_{N1} \approx 3$ K and $T_{N2} \approx 1$ K. A clear Shubnikov-de-Haas (SdH) oscillation was observed at 4 K, demonstrating the strong two-dimensional nature in this material. Below T_{N2} , the SdH oscillation has two frequencies, indicating that the Fermi surface could be slightly modulated due to the second magnetic transition. We also observed a magnetic hysteresis in the SdH oscillation below T_{N1} . Specifically, there is a unique spike in the magnetoresistance at $B \approx 0.6$ T only when the magnetic field is swept from a high enough field (more than 2 T) to zero field.

Published under license by AIP Publishing. <https://doi.org/10.1063/5.0007517>

Research studies on layered materials have attracted much attention over the last decade.^{1,2} This interest was triggered by the discovery of graphene, where not only the polarity but also the density of carriers can be controlled by the electric field.^{3–5} A wide range of materials not only limited to semiconductors,^{6–8} such as insulators,^{9,10} superconductors,^{11–14} and ferromagnetic materials,^{15–19} have been actively studied with the aim of controlling the physical properties or the phase transition temperature by applying the electric field to such thin film devices. More recently, the research field, so-called van der Waals engineering, has become an important stream.^{1,2} The most striking discovery is the superconductivity in twisted bilayer graphene, which is an originally zero gapped semiconductor.²⁰ By stacking a strong spin-orbit transition metal dichalcogenide on a ferromagnetic thin layer, a magnetic skyrmion phase can be induced.²¹ Thus, it is an urgent task to investigate a variety of materials, which can be fabricated into atomically thin films and explore atomically stacked devices with new physical properties. Specifically, magnetic materials could be useful for future spintronic applications.^{22,23}

CeTe₃ is a layered material in the family of rare earth (R) tritellurides, i.e., RTe₃. It is known as a heavy fermion system with a localized $4f^1$ orbital at the Ce³⁺ site. Its crystal structure consists of a NaCl-type CeTe layer, which is responsible for its magnetic properties, separated by two Te sheets, which are responsible for the highly two-dimensional

(2D) electric transport,²⁴ as shown in Fig. 1(a). Due to the highly 2D electrical transport, the material forms an incommensurate charge density wave (CDW) from well above room temperature, which has been studied extensively.^{25–31}

This material is also known to show two magnetic phase transitions at low temperatures.^{24,32–34} The first magnetic transition at $T_{N1} = 3.1$ K is understood to be from a paramagnetic state to an antiferromagnetic (possibly short range ordering) state. In this phase, the magnetic moment at the Ce site is antiferromagnetically coupled and aligned to an easy axis perpendicular to the layer stacking direction. The second magnetic transition is known to be another antiferromagnetic (possibly long range ordering) transition^{24,32} at $T_{N2} = 1.3$ K. Unlike the case of the first transition, a clear peak in the heat capacity has been observed below T_{N2} and the magnetic moment is still aligned to the in-plane direction (called the *non-parallel* easy axis), but different from the easy axis in the first transition.³³ Nevertheless, the details of these magnetic ordering states are poorly understood. Furthermore, there are no reports on thin film transport measurements.

In the present work, we have performed magnetotransport measurements with 30–40 nm thick CeTe₃ devices. We have observed the coexistence of quantum oscillation with unique magnetotransport phenomena. Specifically, a clear Shubnikov-de-Haas (SdH) oscillation was observed in the magnetic field B range of 3–8 T even above T_{N1} ,

demonstrating the existence of a small Fermi surface pocket. Since such a SdH oscillation has never been reported in bulk CeTe_3 , the result reveals its strong 2D nature, which is possibly enhanced by the thin film fabrication. Furthermore, the SdH oscillation has two frequencies below T_{N2} . This could originate from the modification of the Fermi surface due to the second magnetic transition at T_{N2} . We also observed a magnetic hysteresis in the SdH oscillation below T_{N1} . In particular, a sharp resistance peak appears at $B \approx 0.6$ T only when the magnetic field is swept from a high enough magnetic field (more than 2 T) to zero field (see Fig. 3).

Single crystals of CeTe_3 were synthesized in an evacuated quartz tube. The tube was heated up to 900°C and slowly cooled to 550°C over a period of 7 days. To fabricate thin film devices from the bulk CeTe_3 , we used the mechanical exfoliation technique using scotch tapes.^{3–6} It is noted that all the following fabrication processes should be carried out inside a glovebox with an Ar purity of 99.9999% since CeTe_3 is extremely sensitive to ambient air. After the mechanical exfoliation process, many CeTe_3 thin flakes on the scotch tape were transferred onto a thermally oxidized silicon substrate. We then spin-coated polymethyl-methacrylate (PMMA) resist onto the substrate. The substrate was taken out from the glovebox, and electrode patterns were printed using electron beam lithography. After lithography, the substrate was put back into the glovebox again for the development of the resist. The Au electrodes were deposited using electron beam deposition in a vacuum chamber next to the glovebox. Before the deposition of Au, Ar milling was performed to remove the residual resist and any possibly oxidized layers of CeTe_3 . It should be noted that contact resistance varies greatly with electrode material. Au electrodes were

found to have a minimum contact resistance compared to Ti/Au or Cu. In order to avoid further damage in ambient conditions after the fabrication, the device was capped with PMMA shortly after the electrode deposition and the lift-off process. Figure 1(b) shows a scanning electron microscopy (SEM) image of one of the thin film devices.

Electrical transport measurements were performed by the conventional four-probe method using a lock-in amplifier. The device was cooled with a $^3\text{He}/^4\text{He}$ dilution refrigerator down to 0.2 K, and the external magnetic field was applied using a superconducting magnet. The thicknesses of all measured CeTe_3 thin films were confirmed by using a commercially available atomic force microscope after finishing all the electrical measurements.

The resistivity $\rho(T)$ measured with the CeTe_3 thin film device in Fig. 1(b) is plotted as a function of temperature in Fig. 1(c). Although the CeTe_3 structure is half-metallic on its own, the high conductivity between the two Te sheets gives rise to a highly metallic temperature dependence in CeTe_3 .³² There are two resistivity changes in the low temperature region: the first resistivity drop at $T = 2.7$ K and the second resistivity kink structure at $T = 1.3$ K. These behaviors are consistent with the anomalies observed in bulk CeTe_3 resistivity measurements, which correspond to the two magnetic phase transitions at $T_{N1} = 3.1$ K and $T_{N2} = 1.3$ K.^{24,32} The resistivity at room temperature of this device is $81.3 \mu\Omega \cdot \text{cm}$, resulting in the residual resistivity ratio (RRR) of 59.2 with respect to $\rho(T = 1.5 \text{ K})$. This is 1.3 times higher than the previously reported value of 44.9.²⁴ At the lowest temperature ($T = 0.2$ K), RRR reaches a value of 140, indicating that the device is a high-quality single crystal CeTe_3 thin film.

We next performed magnetoresistance measurements up to $B = 8$ T for the temperature range of 0.4–4 K, as shown in Fig. 2(a). The external magnetic field B was applied perpendicular to the plane, i.e., along the b -axis of CeTe_3 and swept from zero to 8 T. A large positive magnetoresistance $\rho_{xx}(B)$ was observed in the low field regime ($B < 1$ T) along with a clear SdH oscillation, which develops from magnetic fields as low as $B = 2$ T in the case of $T = 2$ K. As far as we know, such a quantum oscillation (including the de Haas-van Alphen effect) has never been reported so far even for bulk CeTe_3 although Lei *et al.* have recently reported a SdH oscillation in GdTe_3 thin films.³⁵ This fact is possibly related to much stronger 2D nature in thin films, compared to bulk crystals. Furthermore, the magnetoresistance behavior drastically changes below $T = 0.8$ K, which is below the second magnetic transition temperature T_{N2} .

In order to extract the oscillatory part of the magnetoresistance, the derivative of $\rho_{xx}(B)$ with respect to $1/B$ was obtained numerically. Fast Fourier transform (FFT) was then performed in order to obtain the frequency f of the quantum oscillation. The results are presented in Fig. 2(b). The main oscillation observed at all temperatures corresponds to a frequency of $f_0 = 32.4$ T, which is about two times smaller than that of GdTe_3 .³⁵ Below $T = 0.8$ K, there is an additional oscillation with $f_2 = 11.0$ T, which can be seen as the secondary peak in the FFT spectrum in Fig. 2(b). The frequencies of these oscillations are proportional to the extremal cross-sectional areas of the Fermi surface perpendicular to the applied magnetic field: $S = 2\pi ef/\hbar$, where S is the Fermi surface area, e is the elementary charge, f is the frequency in the unit of T, and \hbar is the reduced Planck constant.³⁶ Using this equation, we obtained the Fermi surface areas of $S_0 = 3.09 \times 10^{13} \text{ cm}^{-2}$ for $f_0 = 32.4$ T and $S_2 = 1.05 \times 10^{13} \text{ cm}^{-2}$ for $f_2 = 11.0$ T. The main oscillation is present even above the two magnetic transition

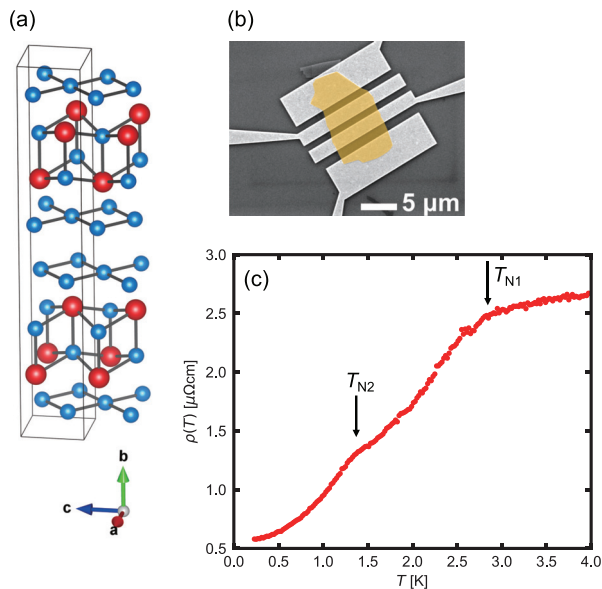


FIG. 1. (a) Crystal structure of CeTe_3 . The red and blue spheres represent Ce and Te atoms, respectively. The black lined box indicates the unit cell, with unit lattice vectors of $a \sim c \sim 4.4 \text{ \AA}$ and $b \sim 26 \text{ \AA}$. (b) SEM image of a typical thin film device. CeTe_3 is shown in yellow (false color). (c) Temperature dependence of the resistivity in the CeTe_3 thin film device. There are two resistivity drops at 2.7 K and 1.3 K, which correspond to the two magnetic transition temperatures T_{N1} and T_{N2} , respectively.

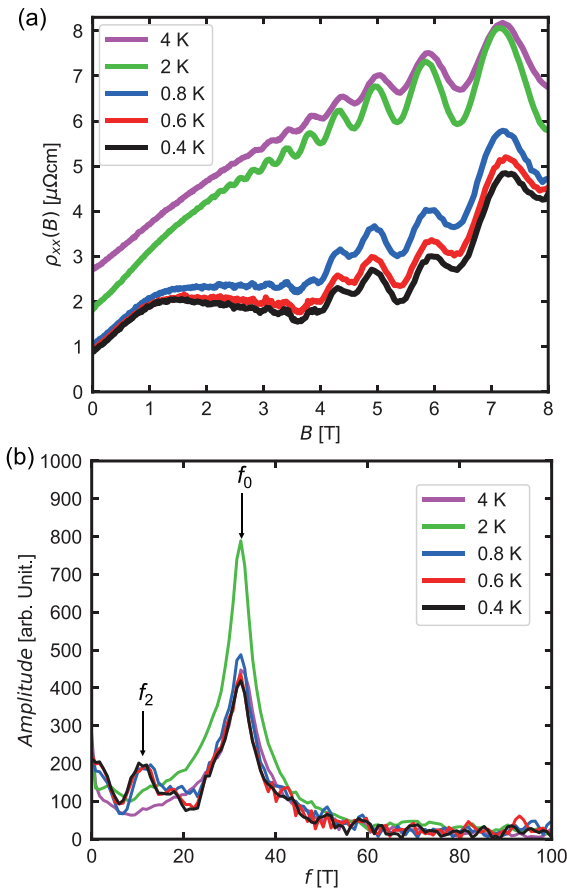


FIG. 2. (a) Magnetoresistance measured with a 40 nm thick CeTe₃ thin film device at several different temperatures. The external magnetic field was applied perpendicular to the plane and swept from zero to 8 T. (b) FFT for the derivative of $\rho_{xx}(B)$ vs $1/B$. The main oscillation peak has been observed at $f_0 = 32.4$ T below 4 K. The secondary oscillation peak has been observed at $f_2 = 11.0$ T only below 0.8 K. The peak at 0 T is due to the DC offset of the frequency.

temperatures, but well below its CDW transition temperature ($T_{CDW} > 500$ K).^{26–29} The origin of this Fermi surface pocket can be attributed to the reconstruction of the Fermi surface due to the incommensurate CDW, which has been observed through photoemission spectroscopy experiments^{26,28} as well as through quantum oscillations of other RTe₃ materials.^{35,37,38}

Although the angular dependence of the SdH oscillation has not been measured in the present study, it was already demonstrated in a similar tritelluride thin film device, i.e., GdTe₃³⁵ where the SdH oscillation follows $1/\cos\theta$ (θ is the angle between the applied magnetic field and the layer stacking direction). This indicates a highly 2D geometry of the Fermi pockets. Since the crystal structure and the high conduction of the Te layers are the same for GdTe₃ and CeTe₃, we believe that the SdH oscillation observed in CeTe₃ also originates from a highly 2D Fermi surface pocket. Specifically, S_0 in the CeTe₃ device is two times smaller than that in a thin film GdTe₃ device, where the effective mass is known to be as small as $\approx 0.1m_0$ (m_0 is the bare electron mass).³⁵ This fact suggests that the conduction electrons between

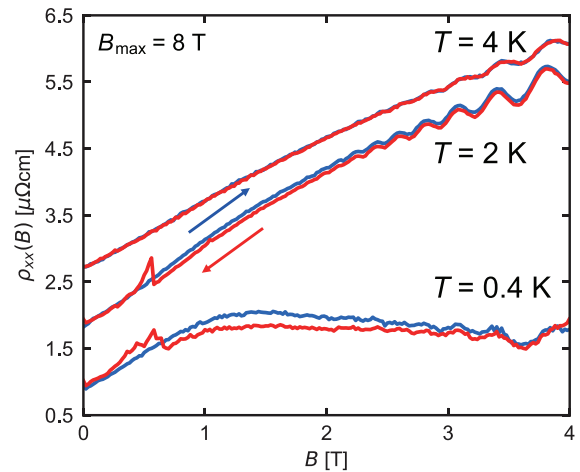


FIG. 3. Hysteresis in magnetoresistance measured at $T = 2$ and 0.4 K. There is a clear hysteresis between the blue and red curves where the magnetic field is swept from 0 to 8 T and from 8 to 0 T, respectively. A clear jump in resistance was observed only for the red curve at $B \approx 0.6$ T. Such a hysteresis was not observed at $T = 4$ K above T_{N1} .

the Te sheets in the CeTe₃ device have a similarly small effective mass. In addition, we detected the secondary oscillation with a frequency of f_2 , which does not exist in GdTe₃ and develops only after the second magnetic transition temperature T_{N2} . According to Ref. 32, the second magnetic transition at T_{N2} is related to a spin density wave transition with formation of heavy quasiparticles. Thus, such reconstruction of the Fermi surface along with this transition could be a possible cause of this new oscillation, but further investigation is required to confirm the hypothesis. We note that these SdH frequencies have also been observed in multiple different CeTe₃ devices, confirming their reproducibility.

In a typical SdH oscillation, the FFT amplitude for a given frequency decreases with increasing temperature. However, FFT amplitudes of the main oscillation remained mostly constant, with the exception at $T = 2$ K. A similar result has been reported in GdTe₃, where the FFT amplitude plateaus below its antiferromagnetic transition temperature, while showing a typical temperature dependence well above the transition temperature.³⁵ Our scenario is consistent with this report; in other words, the unconventional temperature dependence of the FFT amplitude depends strongly on the interaction between the magnetic order at the CeTe site and the conduction electrons.

In addition to the SdH oscillations discussed above, we observed a magnetic hysteresis behavior, superimposed onto the SdH oscillations, below the first antiferromagnetic ordering temperature T_{N1} . This is highlighted in Fig. 3. At 4 K above T_{N1} , there is no hysteresis in the SdH oscillation. Below T_{N1} , however, a clear magnetic hysteresis is observed with a sharp peak structure at $B \approx 0.6$ T. The magnetic hysteresis in the SdH oscillation vanishes above $B \approx 4$ T, and the sharp peak appears only when B is swept from a high enough field (in this case, $B_{max} = 8$ T) to zero field, which we call the negative field sweeping. Note that quantum oscillations with magnetic hysteresis are reproducible for other CeTe₃ thin film devices, even below T_{N2} , and also when the applied magnetic field is negative (see Fig. 4).

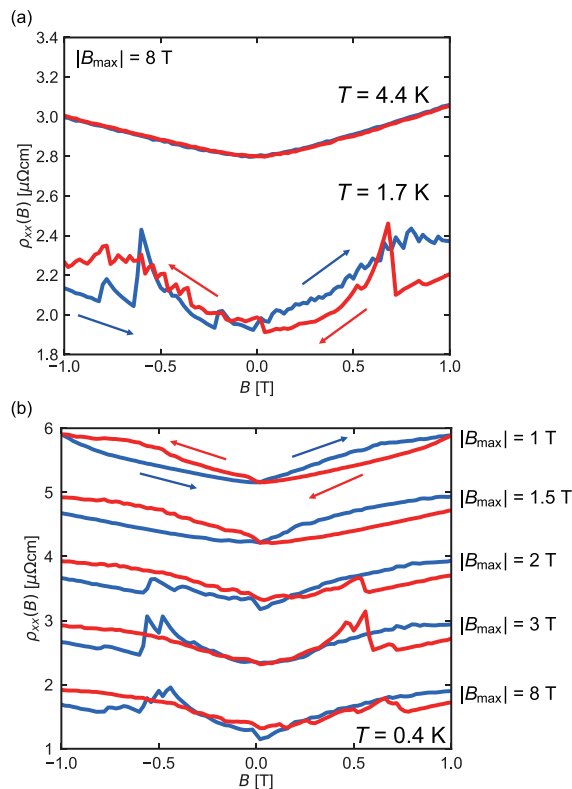


FIG. 4. Measurements performed on a different CeTe_3 device. (a) Magnetoresistance in the field range of ± 1 T measured at $T = 4.4$ and 1.7 K. A similar resistance jump to Fig. 3 was observed at $B \approx \pm 0.6$ T. In this case, $|B_{\text{max}}| = 8$ T. (b) $|B_{\text{max}}|$ dependence of the magnetoresistance in the field range of ± 1 T measured at $T = 0.4$ K. The sharp peak disappears when $|B_{\text{max}}|$ is lower than 1.5 T.

Furthermore, the peak amplitude depends on the absolute value of B_{max} . At $T = 0.4$ K, when $|B_{\text{max}}|$ is lower than 1.5 T, the peak at $B \approx 0.6$ T vanishes, while still preserving the hysteresis behavior, as shown in Fig. 4(b). Such a hysteresis has never been reported previously in bulk CeTe_3 as well as in thin film GdTe_3 devices.³⁵ On the other hand, a hysteresis closely resembling our measurements has been observed for the magnetoresistance measurements in CeTe_2 ,³⁹ a variation of CeTe_3 . CeTe_2 has the same crystal structure as CeTe_3 , but has a single Te layer instead of the double Te layers, and is known to order ferrimagnetically with an easy axis along the layer stacking direction.⁴⁰ This is different from the magnetic order of bulk CeTe_3 , where the magnetic moments at the Ce sites in the two magnetic phases are believed to be aligned to the basal plane.^{32,33} One possible scenario to explain the magnetoresistance hysteresis and peak structure observed in CeTe_3 devices is that by thin film fabrication, we have induced a canting of the magnetic moments along the layer stacking direction, resulting in a similar magnetoresistance effect to CeTe_2 . There is a supportive result where the perpendicular anisotropy of a van der Waals ferromagnet Fe_3GeTe_2 is enhanced by making it atomically thinner.⁴¹ In order to elucidate more details, it would be desirable to perform further experiments in the future on the thickness dependence of the peak structure.

In conclusion, we have performed magnetotransport measurements of $30\text{--}40$ nm thick CeTe_3 thin film devices. A clear SdH oscillation was observed from $T = 4$ K, indicating a highly two-dimensional character of the conduction electrons, possibly enhanced due to thin film fabrication. Below the second magnetic transition temperature $T_{\text{N}2} = 1.3$ K, on the other hand, SdH oscillations with two different frequencies were obtained. The FFT analysis revealed the existence of two small Fermi pockets whose sizes are $3.09 \times 10^{13} \text{ cm}^{-2}$ and $1.05 \times 10^{13} \text{ cm}^{-2}$. In addition, a magnetic hysteresis superimposed to the SdH oscillation was detected below the first antiferromagnetic temperature $T_{\text{N}1} = 2.7$ K. Specifically, a sharp peak at $B \approx 0.6$ T was clearly observed when the magnetic field was swept from the high enough field to zero field. Materials where quantum oscillations and magnetic hysteresis coexist are extremely scarce. Along with the ease of thin film fabrication through mechanical exfoliation, further research on CeTe_3 could pave the way for f -orbital spintronics and could provide an ideal stage for understanding the interplay between electronic quantum conduction and localized heavy fermion spins.

We thank H. Sakai, K. Kuroki, M. Ochi, and K. Deguchi for fruitful discussions. The cell structure of CeTe_3 was visualized using VESTA.⁴² This work was supported by JSPS KAKENHI (Grant Nos. JP16H05964, JP17K18756, JP19K21850, JP20H02557, JP26103002, JP19H00656, and JP19H05826), the Mazda Foundation, the Shimadzu Science Foundation, the Yazaki Memorial Foundation for Science and Technology, the SCAT Foundation, the Murata Science Foundation, the Toyota Riken Scholar, and the Kato Foundation for Promotion of Science.

DATA AVAILABILITY

The data that support the findings of this study are available from the corresponding author upon reasonable request.

REFERENCES

- A. K. Geim and I. V. Grigorieva, *Nature* **499**, 419 (2013).
- K. S. Novoselov, A. Mishchenko, A. Carvalho, and A. H. Castro Neto, *Science* **353**, aac9439 (2016).
- K. S. Novoselov, A. K. Geim, S. V. Morozov, D. Jiang, Y. Zhang, S. V. Dubonos, I. V. Grigorieva, and A. A. Firsov, *Science* **306**, 666 (2004).
- K. S. Novoselov, A. K. Geim, S. V. Morozov, D. Jiang, M. I. Katsnelson, I. V. Grigorieva, S. V. Dubonos, and A. A. Firsov, *Nature* **438**, 197 (2005).
- Y. Zhang, Y.-W. Tan, H. L. Stormer, and P. Kim, *Nature* **438**, 201 (2005).
- K. S. Novoselov, D. Jiang, F. Schedin, T. J. Booth, V. V. Khotkevich, S. V. Morozov, and A. K. Geim, *Proc. Natl. Acad. Sci. U. S. A.* **102**, 10451 (2005).
- B. Radisavljevic, A. Radenovic, J. Brivio, V. Giacometti, and A. Kis, *Nat. Nanotechnol.* **6**, 147 (2011).
- J. T. Ye, Y. J. Zhang, R. Akashi, M. S. Bahramy, R. Arita, and Y. Iwasa, *Science* **338**, 1193 (2012).
- C. R. Dean, A. F. Young, I. Meric, C. Lee, L. Wang, S. Sorgenfrei, K. Watanabe, T. Taniguchi, P. Kim, K. L. Shepard, and J. Hone, *Nat. Nanotechnol.* **5**, 722 (2010).
- L. A. Ponomarenko, A. K. Geim, A. A. Zhukov, R. Jalil, S. V. Morozov, K. S. Novoselov, I. V. Grigorieva, E. H. Hill, V. V. Cheianov, V. I. Fal'ko, K. Watanabe, T. Taniguchi, and R. V. Gorbachev, *Nat. Phys.* **7**, 958 (2011).
- Y. Cao, A. Mishchenko, G. L. Yu, E. Khestanova, A. P. Rooney, E. Prestat, A. V. Kretinin, P. Blake, M. B. Shalom, C. Woods, J. Chapman, G. Balakrishnan, I. V. Grigorieva, K. S. Novoselov, B. A. Piot, M. Potemski, K. Watanabe, T. Taniguchi, S. J. Haigh, A. K. Geim, and R. V. Gorbachev, *Nano Lett.* **15**, 4914 (2015).
- J.-F. Ge, Z.-L. Liu, C. Liu, C.-L. Gao, D. Qian, Q.-K. Xue, Y. Liu, and J.-F. Jia, *Nat. Mater.* **14**, 285 (2015).

- ¹³J. Shiogai, Y. Ito, T. Mitsuhashi, T. Nojima, and A. Tsukazaki, *Nat. Phys.* **12**, 42 (2016).
- ¹⁴Y. Yu, L. Ma, P. Cai, R. Zhong, C. Ye, J. Shen, G. D. Gu, X. H. Chen, and Y. Zhang, *Nature* **575**, 156 (2019).
- ¹⁵C. Gong, L. Li, Z. Li, H. Ji, A. Stern, Y. Xia, T. Cao, W. Bao, C. Wang, Y. Wang, Z. Q. Qiu, R. J. Cava, S. G. Louie, J. Xia, and X. Zhang, *Nature* **546**, 265 (2017).
- ¹⁶B. Huang, G. Clark, E. Navarro-Moratalla, D. R. Klein, R. Cheng, K. L. Seyler, D. Zhong, E. Schmidgall, M. A. McGuire, D. H. Cobden, W. Yao, D. Xiao, P. Jarillo-Herrero, and X. Xu, *Nature* **546**, 270 (2017).
- ¹⁷Z. Wang, T. Zhang, M. Ding, B. Dong, Y. Li, M. Chen, X. Li, J. Huang, H. Wang, X. Zhao, Y. Li, D. Li, C. Jia, L. Sun, H. Guo, Y. Ye, D. Sun, Y. Chen, T. Yang, J. Zhang, S. Ono, Z. Han, and Z. Zhang, *Nat. Nanotechnol.* **13**, 554 (2018).
- ¹⁸Z. Fei, B. Huang, P. Malinowski, W. Wang, T. Song, J. Sanchez, W. Yao, D. Xiao, X. Zhu, A. F. May, W. Wu, D. H. Cobden, J.-H. Chu, and X. Xu, *Nat. Mater.* **17**, 778 (2018).
- ¹⁹Y. Deng, Y. Yu, Y. Song, J. Zhang, N. Z. Wang, Z. Sun, Y. Yi, Y. Z. Wu, S. Wu, J. Zhu, J. Wang, X. H. Chen, and Y. Zhang, *Nature* **563**, 94 (2018).
- ²⁰Y. Cao, V. Fatemi, S. Fang, K. Watanabe, T. Taniguchi, E. Kaxiras, and P. Jarillo-Herrero, *Nature* **556**, 43 (2018).
- ²¹Y. Wu, S. Zhang, G. Yin, J. Zhang, W. Wang, Y. L. Zhu, J. Hu, K. Wong, C. Fang, C. Wan, X. Han, Q. Shao, T. Taniguchi, K. Watanabe, J. Zang, Z. Mao, X. Zhang, and K. L. Wang, *Nat. Commun.* **11**, 3860 (2020).
- ²²T. Song, X. Cai, M. W. Tu, X. Zhang, B. Huang, N. P. Wilson, K. L. Seyler, L. Zhu, T. Taniguchi, K. Watanabe, M. A. McGuire, D. H. Cobden, D. Xiao, W. Yao, and X. Xu, *Science* **360**, 1214 (2018).
- ²³X. Wang, J. Tang, X. Xia, C. He, J. Zhang, Y. Liu, C. Wan, C. Fang, C. Guo, W. Yang, Y. Guang, X. Zhang, H. Xu, J. Wei, M. Liao, X. Lu, J. Feng, X. Li, Y. Peng, H. Wei, R. Yang, D. Shi, X. Zhang, Z. Han, Z. Zhang, G. Zhang, G. Yu, and X. Han, *Sci. Adv.* **5**, eaaw8904 (2019).
- ²⁴Y. Iyeiri, T. Okumura, C. Michioka, and K. Suzuki, *Phys. Rev. B* **67**, 144417 (2003).
- ²⁵E. DiMasi, M. C. Aronson, J. F. Mansfield, B. Foran, and S. Lee, *Phys. Rev. B* **52**, 14516 (1995).
- ²⁶V. Brouet, W. L. Yang, X. J. Zhou, Z. Hussain, N. Ru, K. Y. Shin, I. R. Fisher, and Z. X. Shen, *Phys. Rev. Lett.* **93**, 126405 (2004).
- ²⁷H. J. Kim, C. D. Malliakas, A. T. Tomić, S. H. Tessmer, M. G. Kanatzidis, and S. J. L. Billinge, *Phys. Rev. Lett.* **96**, 226401 (2006).
- ²⁸V. Brouet, W. L. Yang, X. J. Zhou, Z. Hussain, R. G. Moore, R. He, D. H. Lu, Z. X. Shen, J. Laverock, S. B. Dugdale, N. Ru, and I. R. Fisher, *Phys. Rev. B* **77**, 235104 (2008).
- ²⁹C. D. Malliakas and M. G. Kanatzidis, *J. Am. Chem. Soc.* **128**, 12612 (2006).
- ³⁰A. Tomic, Z. Rak, J. P. Veazey, C. D. Malliakas, S. D. Mahanti, M. G. Kanatzidis, and S. H. Tessmer, *Phys. Rev. B* **79**, 085422 (2009).
- ³¹U. Ralević, N. Lazarević, A. Baum, H.-M. Eiter, R. Hackl, P. Giraldo-Gallo, I. R. Fisher, C. Petrovic, R. Gajić, and Z. V. Popović, *Phys. Rev. B* **94**, 165132 (2016).
- ³²K. Deguchi, T. Okada, G. F. Chen, S. Ban, N. Aso, and N. K. Sato, *J. Phys.: Conf. Ser.* **150**, 042023 (2009).
- ³³D. A. Zocco, J. J. Hamlin, T. A. Sayles, and M. B. Maple, *Phys. Rev. B* **79**, 134428 (2009).
- ³⁴R. Okuma, D. Ueta, S. Kuniyoshi, Y. Fujisawa, B. Smith, C. H. Hsu, Y. Inagaki, W. Si, T. Kawae, H. Lin, F. C. Chuang, T. Masuda, R. Kobayashi, and Y. Okada, *Sci. Rep.* (in press), [arXiv:2007.15193](https://arxiv.org/abs/2007.15193).
- ³⁵S. Lei, J. Lin, Y. Jia, M. Gray, A. Topp, G. Farahi, S. Klemen, T. Gao, F. Rodolakis, J. L. McChesney, C. R. Ast, A. Yazdani, K. S. Burch, S. Wu, N. P. Ong, and L. M. Schoop, *Sci. Adv.* **6**, eaay6407 (2020).
- ³⁶I. M. Lifshitz and A. M. Kosevich, *Sov. Phys. JETP* **2**, 636 (1956).
- ³⁷N. Ru, R. A. Borzi, A. Rost, A. P. Mackenzie, J. Laverock, S. B. Dugdale, and I. R. Fisher, *Phys. Rev. B* **78**, 045123 (2008).
- ³⁸A. A. Sinchenko, P. D. Grigoriev, P. Monceau, P. Lejay, and V. N. Zverev, *J. Low Temp. Phys.* **185**, 657 (2016).
- ³⁹M. H. Jung, K. Umeo, T. Fujita, and T. Takabatake, *Phys. Rev. B* **62**, 11609 (2000).
- ⁴⁰J. G. Park, I. P. Swainson, W. J. L. Buyers, M. H. Jung, and Y. S. Kwon, *Physica B* **241–243**, 684 (1997).
- ⁴¹T. Ohta, K. Sakai, H. Taniguchi, B. Driesen, Y. Okada, K. Kobayashi, and Y. Niimi, *Appl. Phys. Express* **13**, 043005 (2020).
- ⁴²K. Momma and F. Izumi, *J. Appl. Cryst.* **44**, 1272–1276 (2011).